Journal of
Synchrotron
Radiation

ISSN 0909-0495

Received 19 November 2010
Accepted 3 October 2011

X-ray photon correlation spectroscopy in systems without long-range order: existence of an intermediate-field regime

Karl Ludwig

Physics Department, Boston University, 590 Commonwealth Avenue, Boston, MA 02215, USA.
E-mail: ludwig@bu.edu

Successful X-ray photon correlation spectroscopy studies often require that signals be optimized while minimizing power density in the sample to decrease radiation damage and, at free-electron laser sources, thermal impact. This suggests exploration of scattering outside the Fraunhofer far-field diffraction limit $d^2/\lambda \ll R$, where d is the incident beam size, λ is the photon wavelength and R is the sample-to-detector distance. Here it is shown that, in an intermediate regime $d^2/\lambda > R \gg d\xi/\lambda$, where ξ is the structural correlation length in the material, the ensemble averages of the scattered intensity and of the structure factor are equal. Similarly, in the regime $d^2/\lambda > R \gg d\xi(\tau)/\lambda$, where $\xi(\tau)$ is a time-dependent dynamics length scale of interest, the ensemble-averaged correlation functions $g_1(\tau)$ and $g_2(\tau)$ of the scattered electric field are also equal to their values in the far-field limit. This broadens the parameter space for X-ray photon correlation spectroscopy experiments, but detectors with smaller pixel size and variable focusing are required to more fully exploit the potential for such studies.

© 2012 International Union of Crystallography
Printed in Singapore – all rights reserved

Keywords: X-ray diffraction; X-ray photon correlation spectroscopy.

1. Introduction

X-ray photon correlation spectroscopy (XPCS) experiments offer unique possibilities to examine equilibrium dynamics and non-equilibrium kinetics in materials on length scales ranging from 10^0 to 10^4 nm (Sutton, 2008). With the continuing development of accelerator-based X-ray sources with ever-higher brilliance, including new generations of storage rings (*e.g.* PETRA-III, NSLS-II), free-electron lasers (LCLS, European XFEL) and energy-recovery linacs (*e.g.* Cornell ERL), the technique's importance will continue to grow. In designing XPCS experiments, several conflicting criteria must be considered. Because studies are usually statistics limited, experiments must carefully maximize coherent scattered intensity while minimizing perturbation to the sample under study, either through radiation damage or thermal spikes due to adiabatic heating from individual pulses at free-electron lasers, particularly LCLS. Source properties and detector pixel size also factor into issues such as choosing incident beam size and sample-to-detector distance. In considering compromises to best achieve these goals, it has been widely assumed that XPCS studies should operate in the Fraunhofer far-field scattering limit with $R \gg d^2/\lambda$, where d is the incident beam size, λ is the photon wavelength and R is the sample-to-detector distance (Born & Wolf, 1999). Here we show that there is an 'intermediate-field' regime between the traditional Fraunhofer far-field and Fresnel near-field regimes in which the scattering is no longer governed by the structure factor, but in which ensemble-averaged scattering and temporal correlations of the scattered electric field bear close correspondence to the quantities measured in a far-field experiment.

2. Scattered intensity and structure factor

2.1. The far-field condition

We begin by reviewing the derivation of the far-field condition. In the scattering geometry of Fig. 1, we have a photon beam of wavevector $\mathbf{k}_{\rm in} = (2\pi/\lambda)\hat{\mathbf{z}} = k\hat{\mathbf{z}}$ and transverse

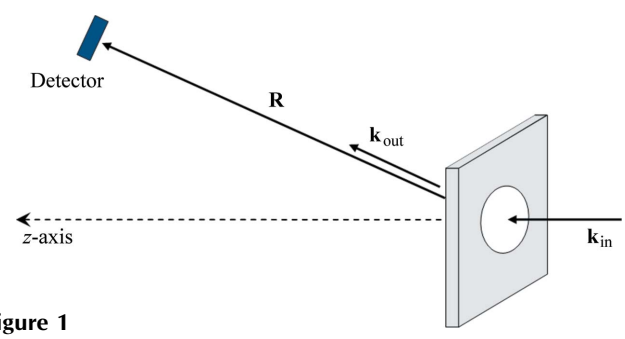

Figure 1
Scattering geometry used in the analysis.

diameter d scattering from a sample of thickness t. We put the origin of our Cartesian coordinate system at the centre of the illuminated volume; the vector from the origin of the coordinate system to the detector is $\mathbf{R} = R\hat{\mathbf{R}}$. Throughout our treatment we ignore effects of finite longitudinal coherence.

For simplicity we assume N point-like scatterers, each with unity scattering power and individual position $\mathbf{r}_i$ referenced to the origin of the coordinate system. The distance from an individual scatterer to the detector is $|\mathbf{R} - \mathbf{r}_i|$ and the intensity recorded per unit solid angle is

$$I = \Big| \sum_i \frac{1}{|\mathbf{R} - \mathbf{r}_i|} \exp\big[ik(|\mathbf{R} - \mathbf{r}_i| + z_i)\big]\Big|^2, \qquad (1)$$

where the term z_i accounts for differences in path length of the *incident* photons. Keeping terms to order kr_i^2/R the argument of the exponent is

$$\begin{aligned} k\big(|\mathbf{R} - \mathbf{r}_i| + z_i\big) &= k\Big[\big(R^2 + r_i^2 - 2\mathbf{R}\cdot\mathbf{r}_i\big)^{1/2} + z_i\Big] \\ &= k\left[R\left(1 + \frac{r_i^2}{R^2} - \frac{2\mathbf{R}\cdot\mathbf{r}_i}{R^2}\right)^{1/2} + z_i\right] \\ &\simeq k\left\{R\left[1 + \frac{r_i^2}{2R^2} - \frac{\mathbf{R}\cdot\mathbf{r}_i}{R^2} - \frac{(\mathbf{R}\cdot\mathbf{r}_i)^2}{2R^4}\right] + z_i\right\} \\ &= k\left(R + \frac{|\mathbf{r}_i \times \hat{\mathbf{R}}|^2}{2R} - \frac{\mathbf{R}\cdot\mathbf{r}_i}{R} + z_i\right) \\ &= k\left(R + \frac{|\mathbf{r}_i \times \hat{\mathbf{R}}|^2}{2R} - \hat{\mathbf{R}}\cdot\mathbf{r}_i + \hat{\mathbf{z}}\cdot\mathbf{r}_i\right) \\ &= kR + \frac{k|\mathbf{r}_i \times \hat{\mathbf{R}}|^2}{2R} - \big(k\hat{\mathbf{R}} - k\hat{\mathbf{z}}\big)\cdot\mathbf{r}_i \\ &= kR + \frac{k|\mathbf{r}_i \times \hat{\mathbf{R}}|^2}{2R} - (\mathbf{k}_{\rm out} - \mathbf{k}_{\rm in})\cdot\mathbf{r}_i \\ &= kR + \frac{k|\mathbf{r}_i \times \hat{\mathbf{R}}|^2}{2R} - \mathbf{q}\cdot\mathbf{r}_i, \end{aligned} \qquad (2)$$

where we have introduced $\mathbf{k}_{\rm out} = (2\pi/\lambda)\hat{\mathbf{R}}$ and the change in wavevector $\mathbf{q} = \mathbf{k}_{\rm out} - \mathbf{k}_{\rm in}$. Considering the denominator in (1), we assume $kd \gg 1$ so that, to order kr_i^2/R we have $|\mathbf{R} - \mathbf{r}_i| \simeq R$. Thus the intensity measured by the detector is

$$\begin{aligned} I &= \left|\sum_i \frac{1}{R}\exp\left(ikR + \frac{ik|\mathbf{r}_i \times \hat{\mathbf{R}}|^2}{2R} - i\mathbf{q}\cdot\mathbf{r}_i\right)\right|^2 \\ &= \left|\sum_i \frac{1}{R}\exp\left(\frac{ik|\mathbf{r}_i \times \hat{\mathbf{R}}|^2}{2R} - i\mathbf{q}\cdot\mathbf{r}_i\right)\right|^2 \\ &\simeq \left|\sum_i \frac{1}{R}\exp(-i\mathbf{q}\cdot\mathbf{r}_i)\right|^2 \equiv \frac{NS(\mathbf{q})}{R^2}, \end{aligned} \qquad (3)$$

where the approximate equality holds if

$$kr_i^2/2R \ll 1. \qquad (4)$$

Since the maximum r_i are of order $d/2$, then this requires for the validity of the 'far-field' condition (*i.e.* that the scattered intensity be proportional to the structure factor)

$$kd^2/8R = \pi d^2/4\lambda R \ll 1, \qquad (5)$$

or, equivalently,

$$R \gg d^2/\lambda. \qquad (6)$$

2.2. Effect of ensemble averaging in materials without long-range order

Consider the consequences of ensemble averaging in a system without long-range order (*i.e.* any correlation length ξ is much smaller than d). If we do not make the far-field assumption, the intensity measured by the detector when averaged over an ensemble of statistically similar systems is

$$\begin{aligned} \langle I\rangle &= \left\langle\left|\sum_i \frac{1}{R}\exp\left(\frac{ik|\mathbf{r}_i \times \hat{\mathbf{R}}|^2}{2R} - i\mathbf{q}\cdot\mathbf{r}_i\right)\right|^2\right\rangle \\ &= \left\langle\sum_{i,j} \frac{1}{R^2}\exp\left[\frac{ik\Big(|\mathbf{r}_i \times \hat{\mathbf{R}}|^2 - |\mathbf{r}_j \times \hat{\mathbf{R}}|^2\Big)}{2R} - i\mathbf{q}\cdot\mathbf{r}_{ij}\right]\right\rangle, \end{aligned} \qquad (7)$$

where $\mathbf{r}_{ij} = \mathbf{r}_i - \mathbf{r}_j$. Terms for $r_{ij} > \xi$ involve uncorrelated atoms and will average to zero except in the forward-scattering direction. The terms for $r_{ij} < \xi$ involve the phase factor,

$$\left|\frac{k\big(|\mathbf{r}_i \times \hat{\mathbf{R}}|^2 - |\mathbf{r}_j \times \hat{\mathbf{R}}|^2\big)}{2R}\right| \le \frac{kd\xi}{R} = \frac{2\pi d\xi}{\lambda R}. \qquad (8)$$

Therefore to find the same ensemble average as obtained in the far-field limit we only require that

$$d\xi/\lambda R \ll 1, \qquad (9)$$

which can be significantly weaker than the general far-field constraint of equation (6).

We can make this argument more concrete by assuming homogeneity and introducing a density function $n(\mathbf{r}_1,\mathbf{r}_2) = \sum_{ij}\delta(\mathbf{r}_1 - \mathbf{r}_i)\delta(\mathbf{r}_2 - \mathbf{r}_j)$ so that

$$\begin{aligned} \langle I\rangle = \frac{1}{R^2}\iint \mathrm{d}V_1\,\mathrm{d}V_2\,\big\langle n(\mathbf{r}_1,\mathbf{r}_2)\big\rangle \\ \times \exp\left[\frac{ik\Big(|\mathbf{r}_1 \times \hat{\mathbf{R}}|^2 - |\mathbf{r}_2 \times \hat{\mathbf{R}}|^2\Big)}{2R} - i\mathbf{q}\cdot\mathbf{r}_{12}\right]. \end{aligned} \qquad (10)$$

If we assume that the sample is homogeneous with average number density n_0, that the ensemble averaged product $\langle n(\mathbf{r}_1,\mathbf{r}_2)\rangle$ depends only on $\mathbf{r}_{12}$, and that correlations decay rapidly as some function $f(\mathbf{r}) \to \exp(-r/\xi)$ as $\mathbf{r} \to \infty$, then

$$\langle n(\mathbf{r}_1,\mathbf{r}_2)\rangle = n_0 f(\mathbf{r}_{12}) + n_0^2, \qquad (11)$$

so that

$$\begin{aligned} \langle I\rangle = \frac{1}{R^2}\iint \mathrm{d}V_1\,\mathrm{d}V_2\,\big[n_0 f(\mathbf{r}_{12}) + n_0^2\big] \\ \times \exp\left[\frac{ik\Big(|\mathbf{r}_1 \times \hat{\mathbf{R}}|^2 - |\mathbf{r}_2 \times \hat{\mathbf{R}}|^2\Big)}{2R} - i\mathbf{q}\cdot\mathbf{r}_{12}\right]. \end{aligned} \qquad (12)$$

For the n_0^2 term we have

$$n_0^2 \iint \mathrm{d}V_1\,\mathrm{d}V_2 \exp\left[\frac{ik\left(|\mathbf{r}_1\times\hat{\mathbf{R}}|^2-|\mathbf{r}_2\times\hat{\mathbf{R}}|^2\right)}{2R}-i\mathbf{q}\cdot\mathbf{r}_{12}\right]=$$
$$n_0^2\left|\int \mathrm{d}V_1 \exp\left(\frac{ik|\mathbf{r}_1\times\hat{\mathbf{R}}|^2}{2R}\right)\exp(-i\mathbf{q}\cdot\mathbf{r}_1)\right|^2. \quad (13)$$

This is the Fourier transform of the function $\exp(ik|\mathbf{r}_1\times\hat{\mathbf{R}}|^2/2R)$; in the far-field limit $kr_1^2/2R \ll 1$ the integral is simply the Fourier transform of the illuminated volume. The inclusion of the phase term going beyond the far-field approximation introduces large Fourier components with wavenumbers up to $kd/8R = \pi d/4\lambda R$. However, for $q \gg \pi d/4\lambda R$, *i.e.* well beyond the forward-scattering region, the transform becomes negligible, as is the case in the far field. This condition is satisfied for points on the detector outside a region of size d, *i.e.* outside a region the size of the incident beam. Thus traditional small-angle X-ray scattering (SAXS) geometries would satisfy this criterion.

The ensemble averaged intensity is

$$\langle I\rangle = (n_0/R^2)\iint \mathrm{d}V_1\,\mathrm{d}V_2\, f(\mathbf{r}_{12}) \times \exp\left[\frac{ik\left(|\mathbf{r}_1\times\hat{\mathbf{R}}|^2-|\mathbf{r}_2\times\hat{\mathbf{R}}|^2\right)}{2R}-i\mathbf{q}\cdot\mathbf{r}_{12}\right]. \quad (14)$$

Since $f(\mathbf{r}) \to \exp(-r/\xi)$ as $r\to\infty$, contributions from large differences between r_1^2 and r_2^2 in the exponential phase factor are cut off. The phase factor is then as given in equation (8); it makes no contribution in the limit of equation (9), so that we obtain

$$\begin{aligned}\langle I\rangle &= (n_0/R^2)\iint \mathrm{d}V_1\,\mathrm{d}V_2\, f(\mathbf{r}_{12})\exp(-i\mathbf{q}\cdot\mathbf{r}_{12})\\ &= (N/R^2)\int \mathrm{d}V_{12}\, f(\mathbf{r}_{12})\exp(-i\mathbf{q}\cdot\mathbf{r}_{12})\\ &= \frac{NS(\mathbf{q})}{R^2}.\end{aligned} \quad (15)$$

Thus we conclude that, outside the forward direction, there is an 'intermediate-field' regime

$$d^2/\lambda > R \gg d\xi/\lambda \quad (16)$$

in which the scattered intensity is no longer proportional to the structure factor but in which the ensemble-averaged scattered intensity $\langle I\rangle$ remains equal to $NS(q)$. We can understand this simply. If we think of scattering from any particular atom i into the detector as occurring with some 'local' wavenumber change q_i that depends on both the position of the atom in the sample and the position of the detector, then the far-field condition effectively requires that the spread in these 'local' wavenumbers $\Delta q \simeq kd/R$ must be much less than the lowest wavenumber frequency associated with the scale of the illuminated volume, $2\pi/d$. For systems with only short-range order, however, the limit of equation (9) requires only that Δq be much less than the lowest wavenumber frequency associated with structural correlations, $2\pi/\xi$.

3. Temporal correlation functions in systems without long-range order

3.1. Intensity autocorrelation function from homodyne experiments

The time-averaged normalized autocorrelation function of the measured intensity is

$$\frac{\langle I(t)I(t+\tau)\rangle_t}{I_0^2}=\frac{\langle I(0)I(\tau)\rangle}{I_0^2} \quad (17)$$

where

$$I_0=\langle I(t)\rangle_t=\langle I(t)\rangle. \quad (18)$$

The first averages are over time but the second equality assumes ergodicity so that the time average is replaced by an ensemble average.

Within the approximation of equation (2), the cross term in (17) is

$$\begin{aligned}\langle I(0)I(\tau)\rangle &= \frac{1}{R^4}\left\langle \sum_{i,j}\exp\left\{\frac{ik\left(|\mathbf{r}_i(0)\times\hat{\mathbf{R}}|^2-|\mathbf{r}_j(0)\times\hat{\mathbf{R}}|^2\right)}{2R}\right.\right.\\ &\quad\left.-i\mathbf{q}\cdot\left[\mathbf{r}_i(0)-\mathbf{r}_j(0)\right]\right\}\\ &\quad\times\sum_{l,m}\exp\left\{\frac{ik\left(|\mathbf{r}_l(\tau)\times\hat{\mathbf{R}}|^2-|\mathbf{r}_m(\tau)\times\hat{\mathbf{R}}|^2\right)}{2R}\right.\\ &\quad\left.\left.-i\mathbf{q}\cdot\left[\mathbf{r}_l(\tau)-\mathbf{r}_m(\tau)\right]\right\}\right\rangle\\ &= \frac{1}{R^4}\left\langle \sum_{i,j,l,m}\exp\left\{\frac{ik\left(|\mathbf{r}_i(0)\times\hat{\mathbf{R}}|^2-|\mathbf{r}_m(\tau)\times\hat{\mathbf{R}}|^2\right)}{2R}\right.\right.\\ &\quad\left.-i\mathbf{q}\cdot\left[\mathbf{r}_i(0)-\mathbf{r}_m(\tau)\right]\right\}\\ &\quad\times\exp\left\{-\frac{ik\left(|\mathbf{r}_j(0)\times\hat{\mathbf{R}}|^2-|\mathbf{r}_l(\tau)\times\hat{\mathbf{R}}|^2\right)}{2R}\right.\\ &\quad\left.\left.+i\mathbf{q}\cdot\left[\mathbf{r}_j(0)-\mathbf{r}_l(\tau)\right]\right\}\right\rangle.\end{aligned} \quad (19)$$

Following the treatment of §2, we can introduce a density function $n(\mathbf{r}_1,\mathbf{r}_2,\mathbf{r}_3,\mathbf{r}_4,\tau)=\sum_{ijlm}\delta[\mathbf{r}_1-\mathbf{r}_i(0)]\delta[\mathbf{r}_2-\mathbf{r}_j(0)]\delta[\mathbf{r}_3-\mathbf{r}_l(\tau)]\delta[\mathbf{r}_4-\mathbf{r}_m(\tau)]$. The position of particles in the sum will be correlated only if the positions differ by less than some time-dependent length scale $\xi(\tau)$. We therefore expect that

$$\langle n(\mathbf{r}_1,\mathbf{r}_2,\mathbf{r}_3,\mathbf{r}_4,\tau)\rangle = n_0^3 f(\mathbf{r}_{12},\mathbf{r}_{13},\mathbf{r}_{14},\mathbf{r}_{23},\mathbf{r}_{24},\mathbf{r}_{34},\tau)+n_0^4, \quad (20)$$

where, for instance, $f(\mathbf{r}_{12},\mathbf{r}_{13},\mathbf{r}_{14},\mathbf{r}_{23},\mathbf{r}_{24},\mathbf{r}_{34},\tau)\to f'(\mathbf{r}_{12},\mathbf{r}_{13},\mathbf{r}_{23},\mathbf{r}_{24},\mathbf{r}_{34},\tau)+cn_0\exp[-r_{14}/\xi(\tau)]$ as $r_{14}\to\infty$, with c a constant that depends on the illuminated volume geometry. Similar relationships exist for the other terms. Equation (19) can be written

$$\langle I(0)I(\tau)\rangle = \frac{1}{R^4}\iiiint \mathrm{d}V_1\,\mathrm{d}V_2\,\mathrm{d}V_3\,\mathrm{d}V_4\,\langle n(\mathbf{r}_1,\mathbf{r}_2,\mathbf{r}_3,\mathbf{r}_4,\tau)\rangle \times \exp\left[\frac{ik\left(|\mathbf{r}_1\times\hat{\mathbf{R}}|^2-|\mathbf{r}_4\times\hat{\mathbf{R}}|^2\right)}{2R}-i\mathbf{q}\cdot(\mathbf{r}_1-\mathbf{r}_4)\right] \times \exp\left[-\frac{ik\left(|\mathbf{r}_2\times\hat{\mathbf{R}}|^2-|\mathbf{r}_3\times\hat{\mathbf{R}}|^2\right)}{2R}+i\mathbf{q}\cdot(\mathbf{r}_2-\mathbf{r}_3)\right]. \quad (21)$$

As with equation (13) above, the term with n_0^4 is negligible for $q \gg \pi d/4\lambda R$, *i.e.* well beyond the forward-scattering region. Then

$$\langle I(0)I(\tau)\rangle = \frac{n_0^3}{R^4}\iiiint \mathrm{d}V_1\,\mathrm{d}V_2\,\mathrm{d}V_3\,\mathrm{d}V_4\,f(\mathbf{r}_{12},\mathbf{r}_{13},\mathbf{r}_{14},\mathbf{r}_{23},\mathbf{r}_{24},\mathbf{r}_{34},\tau) \times \langle n(\mathbf{r}_1,\mathbf{r}_2,\mathbf{r}_3,\mathbf{r}_4,\tau)\rangle \times \exp\left[\frac{ik\left(|\mathbf{r}_1\times\hat{\mathbf{R}}|^2-|\mathbf{r}_4\times\hat{\mathbf{R}}|^2\right)}{2R}-i\mathbf{q}\cdot(\mathbf{r}_1-\mathbf{r}_4)\right] \times \exp\left[-\frac{ik\left(|\mathbf{r}_2\times\hat{\mathbf{R}}|^2-|\mathbf{r}_3\times\hat{\mathbf{R}}|^2\right)}{2R}+i\mathbf{q}\cdot(\mathbf{r}_2-\mathbf{r}_3)\right]. \quad (22)$$

The correlation function f limits the phase factor contributions to those atomic pairs with $r_{ij} < \xi(\tau)$. As with equation (7), phase factors such as $k(|\mathbf{r}_1\times\hat{\mathbf{R}}|^2-|\mathbf{r}_4\times\hat{\mathbf{R}}|^2)/2R$ will be negligible if $d\xi(\tau)/\lambda R \ll 1$. Because of the assumed homogeneity of the sample, phase factors such as $k(|\mathbf{r}_1\times\hat{\mathbf{R}}|^2+|\mathbf{r}_3\times\hat{\mathbf{R}}|^2)/2R$ will again be negligible for $q \gg \pi d/4\lambda R$.

Thus, within these limits,

$$\begin{aligned}\langle I(0)I(\tau)\rangle &= \frac{n_0^3}{R^4}\iiiint \mathrm{d}V_1\,\mathrm{d}V_2\,\mathrm{d}V_3\,\mathrm{d}V_4 \times f(\mathbf{r}_{12},\mathbf{r}_{13},\mathbf{r}_{14},\mathbf{r}_{23},\mathbf{r}_{24},\mathbf{r}_{34},\tau) \times \exp\left[i\mathbf{q}\cdot(\mathbf{r}_1-\mathbf{r}_4)\right]\exp\left[-i\mathbf{q}\cdot(\mathbf{r}_2-\mathbf{r}_3)\right]\\ &= \frac{1}{\mathrm{R}^4}\iiiint \mathrm{d}V_1\,\mathrm{d}V_2\,\mathrm{d}V_3\,\mathrm{d}V_4\,\langle n(\mathbf{r}_1,\mathbf{r}_2,\mathbf{r}_3,\mathbf{r}_4,\tau)\rangle \times \exp\left[-i\mathbf{q}\cdot(\mathbf{r}_1-\mathbf{r}_4)\right]\exp\left[-i\mathbf{q}\cdot(\mathbf{r}_2-\mathbf{r}_3)\right]\\ &= \frac{N^2\langle S(q,0)S(q,\tau)\rangle}{R^4} \end{aligned} \quad (23)$$

and

$$\frac{\langle I(t)I(t+\tau)\rangle_t}{I_0^2} = \frac{\langle I(t)I(t+\tau)\rangle}{I_0^2} = \frac{\langle S(q,t)S(q,t+\tau)\rangle}{S_0^2(q)} = g_2(\tau). \quad (24)$$

3.2. Intensity autocorrelation function in heterodyne experiments

In a heterodyne experiment the intensity measured is

$$I \propto \left|E_{\mathrm{ref}}+E_{\mathrm{scat}}\right|^2 \cong \left|E_{\mathrm{ref}}\right|^2 + 2\mathrm{Re}(E_{\mathrm{ref}}^*E_{\mathrm{scat}}), \quad (25)$$

where E_{ref} is the electric field from a reference, E_{scat} is the electric field scattered by the sample, and we assume, as usual, that $E_{\mathrm{ref}} \gg E_{\mathrm{scat}}$. If we neglect the stationary intensity from the reference, the time-averaged normalized autocorrelation of the intensity is then

$$\left\langle I(t)I(t+\tau)\right\rangle_t = \left\langle I(t)I(t+\tau)\right\rangle \propto 2I_{\mathrm{ref}}\mathrm{Re}\left\langle E_{\mathrm{scat}}^*(0)E_{\mathrm{scat}}(\tau)\right\rangle. \quad (26)$$

Within the approximation of equation (2), the correlation of interest is

$$\begin{aligned}E_{\mathrm{scat}}^*(0)E_{\mathrm{scat}}(\tau) &= \frac{1}{R^2}\left\langle \sum_i \exp\left[-\frac{ik|\mathbf{r}_i(0)\times\hat{\mathbf{R}}|^2}{2R}+i\mathbf{q}\cdot\mathbf{r}_i(0)\right] \times \sum_j \exp\left[\frac{ik|\mathbf{r}_j(\tau)\times\hat{\mathbf{R}}|^2}{2R}-i\mathbf{q}\cdot\mathbf{r}_j(\tau)\right]\right\rangle\\ &= \frac{1}{R^2}\sum_{i,j}\exp\left\{\frac{ik\left[|\mathbf{r}_j(\tau)\times\hat{\mathbf{R}}|^2-|\mathbf{r}_i(0)\times\hat{\mathbf{R}}|^2\right]}{2R} - i\mathbf{q}\cdot\left[\mathbf{r}_j(\tau)-\mathbf{r}_i(0)\right]\right\}. \end{aligned} \quad (27)$$

By the same arguments used above, in the limits of equation (9) this reduces to $\sum_{ij}\exp\{-i\mathbf{q}\cdot[\mathbf{r}_j(\tau)-\mathbf{r}_i(0)]\} = NF(\mathbf{q},\tau)$, where $F(\mathbf{q},\tau)$ is the intermediate scattering function (Berne & Pecora, 2000).

3.3. Speckle size

The intensity at a given point on the detector depends on the differences in path lengths of photons scattered from different parts of the sample. The maximum difference in path length will occur for scattering from opposite ends of the sample. Within the approximation of equation (2), this maximum difference in phase factors is then

$$\begin{aligned}k\Delta l_{\max} &\simeq \frac{k}{2R}\left[\left(\frac{d}{2}\right)^2-\left(\frac{-d}{2}\right)^2\right]-q\left[\left(\frac{d}{2}\right)-\left(\frac{-d}{2}\right)\right]\\ &= -qd. \end{aligned} \quad (28)$$

The detector intensity will fundamentally change when $k\Delta l_{\max} \simeq 2\pi$, so that within the approximation of equation (2) the speckle size is given by $\Delta q \simeq 2\pi/d$ and the speckle size on the detector is $\Delta x \simeq R\lambda/d$, as is the case within the far-field approximation.

4. Simulations

In order to verify the validity of the results above, (1 + 1) dimensional simulations were performed. Fig. 2 shows how the exact scattering speckle profile of equation (1) changes as a function of detector distance for 10^3 randomly placed point scatterers in a 300 µm beam of 8 keV photons. The two calculations shown are both for an average wavenumber of 1 nm^{-1}. For large distances (R = 5000 m), the calculated structure factor speckle pattern from a given configuration agrees well with the actual calculated intensity. However, for detector distances shorter than the far-field limit of equation

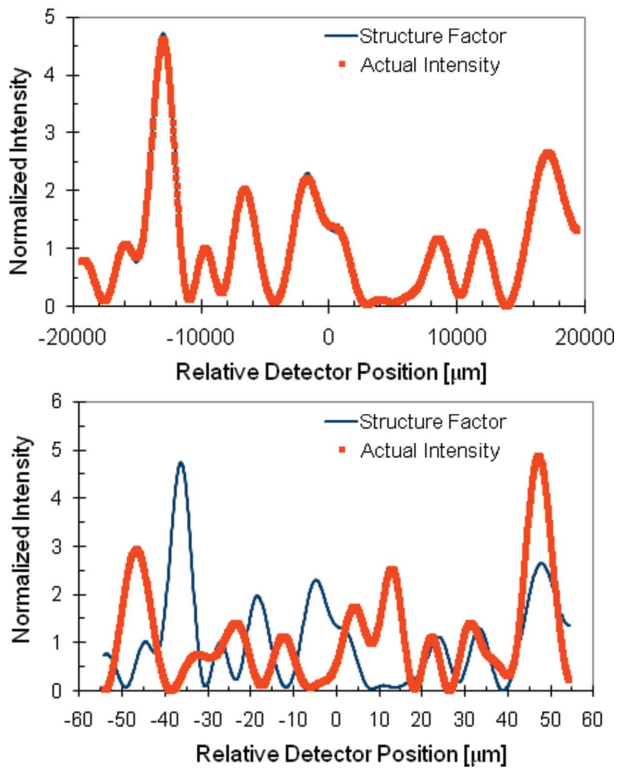

Figure 2
Actual calculated intensity (red) and structure factor (blue) of randomly placed point scatterers in a 300 μm beam for detector distances R = 5000 m (top) and R = 14 m (bottom).

(5) (which is approximately 450 m in this case), the structure factor calculation diverges strongly from the actual speckle profile. As discussed above, the spatial size of the speckles is still approximately $\lambda R/d$. This ranges from 2500 μm for R = 5000 m to 7 μm for R = 14 m. These calculated numbers are in good agreement with what is observed in the figure.

Although the actual speckle intensity is quite different than that predicted by the structure factor when the detector is closer than the far-field limit, the ensemble average of the structure factor and the actual calculated intensity are equal, as suggested by the calculations of §2. Fig. 3 shows the structure factor and actual calculated intensities for an ensemble of 10^2 configurations, each with 10^6 point 'hard sphere' particles maintaining exclusion zones to create short-range order. These calculations used a beam size of 300 μm, a detector

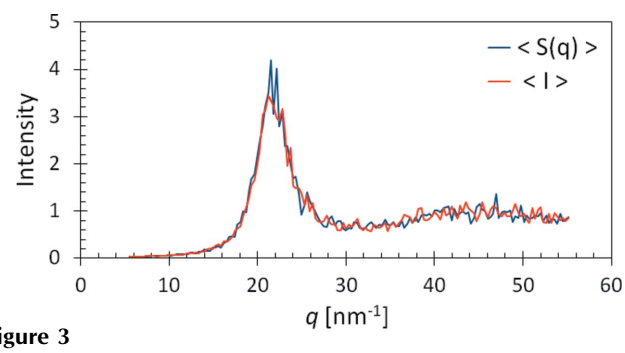

Figure 3
Normalized ensemble-averaged intensity $\langle I \rangle$ (red) and structure factor $\langle S(q) \rangle$ (blue) for 'hard-sphere' particles.

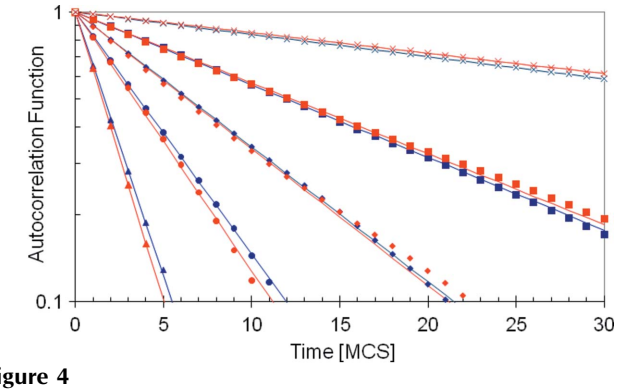

Figure 4
Autocorrelation functions of intensity (red) and $S(q)$ (blue) for random walkers at different wavenumbers.

distance of 5 m and a photon energy of 8 keV. As expected from the results of §2, the agreement is good.

In order to examine the use of homodyne XPCS in the intermediate-field regime, a simulation was performed with 10^3 random walkers taking possible steps of 1 nm in each Monte Carlo step (MCS). Typically runs of 2048 MCS are used. In cases presented here, the beam size is again taken to be 300 μm, the beam energy to be 8 keV and the detector distance 5 m. The simulations examined wavenumbers of 0.25–1.5 nm^{-1}. Fig. 4 compares the normalized autocorrelation functions obtained at different wavenumbers for both the structure factor $S(q)$ and the actual scattering intensity. The symbols are simulated values and the lines are simple fits to an exponential decay. As can be seen, the decay of the autocorrelation function of the actual scattering intensity is very similar to that of the structure factor. For both the structure factor and the actual intensity autocorrelation functions, the decay rate $\tau(q)$ is proportional to q^2, as seen in Fig. 5, and the slopes are similar, giving similar diffusion constants.

5. XPCS experiment strategies

5.1. General considerations

As discussed in the *Introduction*, a fundamental constraint on XPCS studies is the need to maximize their signal-to-noise ratio (SNR) while minimizing perturbation of the sample

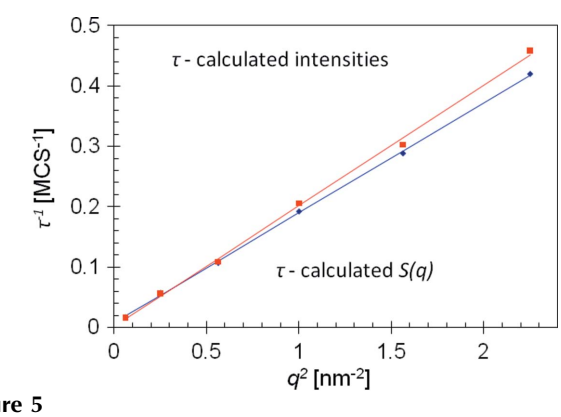

Figure 5
Inverse correlation times τ^{-1} for autocorrelation of calculated intensity (red) and structure factor $S(q)$ (blue) as a function of q^2.

under study, either through radiation damage or thermal spikes owing to adiabatic heating from individual pulses at free-electron lasers, particularly LCLS.

At synchrotron sources, the inherent transverse coherence length is $\zeta = R'/k\sigma$, where σ is the source size and R' is the distance from source to sample. At the planned NSLS-II coherent hard X-ray (CHX) beamline, the inherent vertical coherence length at the sample position is approximately 277 µm and the horizontal coherence length is approximately 31 µm (Fluerasu, 2009). However, coherence lengths larger than about 10 µm produce speckle sizes that are too small to be used effectively with current CCD X-ray detectors. For example, in the planned CHX hutch with a maximum sample–detector distance of 15 m for SAXS studies and approximately 2 m for wide-angle X-ray scattering (WAXS) studies, use of a beam with d = 277 µm would give speckles of size 8 µm and 1 µm for SAXS and WAXS, respectively. In contrast, most CCD X-ray detectors have pixel sizes of 20 µm and larger. Moreover, the sample–detector distance required to reach the far field for a 277 µm beam is almost 500 m. At X-ray FEL sources the beam can be even larger. For instance, at the X-ray correlation spectroscopy (XCS) station being built at LCLS, the unfocused X-ray beam size is approximately 500 µm. To decrease the effective coherence lengths, and better match the vertical and horizontal lengths, synchrotron beamlines often use focusing to create a secondary source. This, however, results in increased X-ray energy density in the sample, potentially exacerbating beam damage problems in soft materials. Focusing the unprecedented peak beam brilliance of XFELs even further exacerbates concerns of sample damage and heating.

As noted by Falus *et al.* (2006), it is highly desirable for X-ray detectors to be developed with smaller pixel sizes to take advantage of the inherently large coherence lengths from current synchrotron sources, particularly in the vertical direction. Using unfocused or less-focused beam would potentially decrease sample damage. When detectors with smaller pixel sizes do become available for XPCS studies of materials with short-range structural order, scattering with an incident beam even as large as several hundred micrometres would still place XPCS experiments well within the intermediate-field range identified in this work, guaranteeing that experiments will give the proper ensemble-averaged result.

As discussed by Falus *et al.* (2006), in a conventional homodyne experiment the SNR is approximately $\beta\langle I\rangle[NM/(1+\beta)]^{1/2}$, where $\langle I\rangle$ is the mean number of photons counted per pixel in each time bin, N is the number of pixels which can be averaged over, M is the number of time bins, and the optical contrast is

$$\beta = \frac{\langle I^2\rangle}{\langle I\rangle^2} - 1. \tag{29}$$

The contrast is reduced by imperfect effective source coherence and by the non-zero range of scattering angles over which the detector integrates. In the far-field case, Lumma *et al.* (2000) have shown that the optical contrast is approximately equal to the product of contrast factors in the x- and y-directions. They calculate the factor in integral form [equation (A9) of Lumma *et al.* (2000)] and give an analytical approximation [equation (A11) of Lumma *et al.* (2000)]. Their integral derivation remains accurate in the intermediate-field regime of equation (16). Parenthetically, however, we note that their analytical approximation underestimates the optical contrast as compared with calculations using the integral; in low-contrast situations it is a factor of $2^{1/2}$ smaller in each direction.

5.2. Fixed number of detector pixels at XFEL sources

For simplicity we assume that the beam dimensions are the same in the x- and y-directions, that the detector pixel sizes are also the same in the two directions and that the beam intensity is constant across its width. We initially assume that the number of pixels N is fixed and that the beam is unfocused and defined by slits to a square of size d. The mean number of photons counted in each time bin in each pixel $\langle I\rangle$ is proportional to d^2a^2/R^2, where a is the pixel size. Using equation (A9) of Lumma *et al.* (2000) for the optical contrast, we therefore seek to maximize the function

$$\frac{\beta\langle I\rangle}{(1+\beta)^{1/2}} = \frac{\left[(2/d^2)\int_0^d \mathrm{d}x\,(d-x)\frac{\sin^2(Sx/2)}{(Sx/2)^2}\right]^2 (da/R)^2}{\left\{1+\left[(2/d^2)\int_0^d \mathrm{d}x\,(d-x)\frac{\sin^2(Sx/2)}{(Sx/2)^2}\right]^2\right\}^{1/2}} = \frac{w^2}{k^2}\frac{\left[(2/w^2)\int_0^w \mathrm{d}v\,(w-v)\frac{\sin^2(v/2)}{(v/2)^2}\right]^2}{\left\{1+\left[(2/w^2)\int_0^w \mathrm{d}v\,(w-v)\frac{\sin^2(v/2)}{(v/2)^2}\right]^2\right\}^{1/2}} \tag{30}$$

where $S = ka/R$ and $w = kad/R$. A normalized plot of the function is shown in Fig. 6. Also shown is the calculated optical contrast β owing to the integration of the scattered intensity over each detector pixel. The SNR improves with increasing w. However, β continuously decreases and, from a practical point of view, Falus *et al.* (2006) suggest that uncertainty in the baseline could be problematic for very small contrasts.

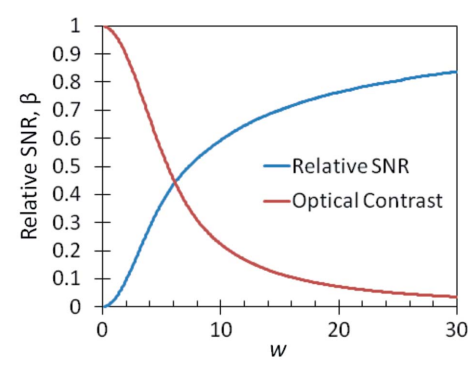

Figure 6
Calculated relative SNR and optical contrast β as a function of the parameter $w = kad/R$ for an XFEL experiment using a fixed number of detector pixels.

Therefore it is probably reasonable to choose some intermediate value for w. With $w = 10$, the SNR is approximately 53% of its optimal value and the optical contrast owing to the lateral coherence factors is 0.22. Using a detector with 20 µm pixels at the XCS station with $R = 5$ m, this corresponds to an incident beam size of approximately 60 µm giving a speckle size of approximately 13 µm. However, a similar SNR and optical contrast can be achieved for this same detector operating at a detector distance of 1 m with a beam size of only 12 µm. While the former example would be in the intermediate-field regime, the latter would be at the transition to the far-field regime. Thus, the variable $w = kad/R$ governs the SNR and permits extensive trade-off between beam size and sample–detector distance.

Focusing the beam to a width d (instead of slitting it) can potentially significantly improve the SNR. If we assume for simplicity that the entire incident beam is focused without loss and that the contrast factor for a coherent focused beam is the same as for a parallel beam (since each point in the illuminated sample volume maintains a well defined phase relationship to other points), then the function which must be maximized for the optimal SNR is equation (30) divided by a factor of d^2. This is optimized by minimizing d. If the detector pixel size a is set, then the smallest possible sample–detector distance R consistent with the wavevector range desired and the intermediate regime identified in this work would maximize w and hence the SNR as shown in Fig. 6. However, again a moderate value of R may instead be desired to provide reasonable contrast.

5.3. Fixed detection solid angle at XFEL sources

In SAXS experiments it is often possible to cover the full range of scattering solid angle Ω defining a given reciprocal space region of interest. WAXS experiments may also be effectively limited to a fixed solid angle by the scattering geometry and the photon wavelength. In these cases $N = \Omega R^2/a^2$ and, in the unfocused case where slits are used to define d, we seek to maximize the function

$$\frac{\beta N^{1/2}\langle I\rangle}{(1+\beta)^{1/2}} = \frac{\left[(2/d^2)\int_0^d \mathrm{d}x\,(d-x)\frac{\sin^2(Sx/2)}{(Sx/2)^2}\right]^2 (\Omega R^2/a^2)^{1/2}(a^2d^2/R^2)}{\left\{1+\left[(2/d^2)\int_0^d \mathrm{d}x\,(d-x)\frac{\sin^2(Sx/2)}{(Sx/2)^2}\right]^2\right\}^{1/2}}$$
$$= \frac{wd\,\Omega^{1/2}}{k}\frac{\left[(2/w^2)\int_0^w \mathrm{d}v\,(w-v)\frac{\sin^2(v/2)}{(v/2)^2}\right]^2}{\left\{1+\left[(2/w^2)\int_0^w \mathrm{d}v\,(w-v)\frac{\sin^2(v/2)}{(v/2)^2}\right]^2\right\}^{1/2}}. \quad (31)$$

For a given value of d, this function is optimized when $w \simeq 6$, so that the detector pixel size is approximately equal to the speckle size. From a practical point of view, limits of detector pixel size and sample–detector distances limit the ability to achieve the optimal value $w \simeq 6$ for large d. A plot of the optimal value of equation (31) as a function of beam diameter d is shown in Fig. 7; it uses values/limits appropriate for SAXS at the XCS station and for typical CCD X-ray detectors: $E = 8$ keV, $a_{\min} = 20$ µm and $R_{\max} = 14$ m. Also shown in Fig. 7 is the calculated optical contrast β and the optimal a/R ratio within the constraints imposed by the above values. For this combination of detector pixel size and maximum sample–detector distance, the ideal $w = 6$ condition can be fulfilled for beam diameters smaller than approximately 100 µm. The SNR continues to improve with increasing d beyond this size, but more slowly and with decreasing optical contrast. It is noteworthy that a beam diameter of 100 µm would require a sample–detector distance of over 60 m to reach the far field, so that experiments would be in the intermediate-field regime identified in this work.

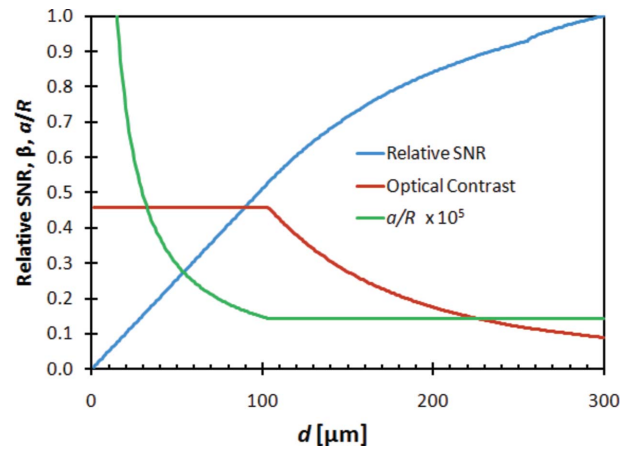

Figure 7
Calculated relative SNR, optical contrast β and a/R ratio (multiplied by a factor of 10^5) as a function of beam size d for an optimized XFEL SAXS experiment measuring scattering into a fixed solid angle. A minimum detector pixel size of 20 µm and maximum sample–detector distance of 14 m is assumed.

If the beam is focused so that it has size d at the sample, the SNR function to be optimized is equation (31) divided as before by a factor of d^2. For a given value of d, the optimal value for the a/R ratio and resulting optical contrast can still be read from Fig. 7. For strong focusing of the entire beam to a few tens of micrometres or less, a SNR gain of an order of magnitude or larger is potentially possible.

6. Conclusions

We have seen that XPCS experiments can be performed in a well defined intermediate-field regime in addition to the traditional far-field regime. This expands the space of possible experimental parameters. However, for a given experiment, trade-offs between sample damage/heating, focusing, incident beam size, detector pixel size, number of detector pixels, reciprocal space range of interest and sample–detector distance need to be carefully considered to optimize the SNR. While the presence of the intermediate-field regime of scattering allows larger beam sizes to be used than are possible

within the usual far-field criterion, detector pixel sizes are currently a significant limitation.

I thank Professor M. Sutton of McGill University for many fruitful discussions. This work was supported by the Department of Energy, Basic Energy Sciences through grant DE-FG02-03ER46037.

References

Berne, B. & Pecora, R. (2000). *Dynamic Light Scattering: With Applications to Chemistry, Biology and Physics.* New York: Dover.

Born, M. & Wolf, E. (1999). *Principles of Optics: Electromagnetic Theory of Propagation, Interference and Diffraction of Light.* Cambridge University Press.

Falus, P., Lurio, L. B. & Mochrie, S. G. J. (2006). *J. Synchrotron Rad.* **13**, 253–259.

Fluerasu, A. (2009). *Conceptual Design Report of the Coherent Hard X-ray Beamline at NSLS-II*, Report LT-XFD_CDR_XPD-00118, Brookhaven National Laboratory, Upton, NY, USA (http://www.bnl.gov/nsls2/docs/PDF/cdr/1_CHX-10-1final.pdf).

Lumma, D., Lurio, L., Mochrie, S. & Sutton, M. (2000). *Rev. Sci. Instrum.* **71**, 3274–3289.

Sutton, M. (2008). *C. R. Phys.* **9**, 657–667.